MICROSTRUCTURES OF CI-CHONDRITE PYRRHOTITE AND CUBANITE. E. L. Berger[1], T. J. Zega[2], and D. S. Lauretta[1]. [1]Lunar and Planetary Laboratory, University of Arizona, Tucson AZ 85721 USA. [2]Naval Research Laboratory, Washington DC, 20375 USA. (elberger@lpl.arizona.edu).

Introduction: CI-chondrite mineralogy is dominated by a fine-grained phyllosilicate matrix, which is host to carbonates, sulfates, sulfides, and magnetite [1, and references therein]. The sulfide minerals troilite (FeS), pentlandite [$(Fe,Ni)_9S_8$], pyrrhotite [$(Fe,Ni)_{1-x}S$], and cubanite ($CuFe_2S_3$) have been reported in CI chondrites; Fe-deficient pyrrhotite is the most common [1]. To date, cubanite has been reported in the CI chondrites Alais, Orgueil, and Ivuna [1, 2]. Cubanite has not been found in any other chondritic sample, but it has been reported in the Stardust collection [3]. Detailed characterization of the crystal structures of CI-chondrite pyrrhotite and cubanite constrains parent-body alteration conditions. We have initiated a microstructural investigation of sulfides in CI chondrites. Here we report the crystal structures and compositions of cubanite and pyrrhotite.

Samples and Analytical Techniques: Eight thin sections of Orgueil were prepared from samples provided by the Vatican Observatory. Fourteen individual cubanite grains and two cubanite/pyrrhotite assemblages from these thin sections were characterized on a Cameca SX-50 electron microprobe at the University of Arizona. Electron-transparent cross sections of two assemblages were prepared at the Naval Research Laboratory (NRL) using an FEI Nova 600 focused ion beam-scanning electron microscope (FIB-SEM) based on previously described methods [4]. Assemblages E3 (an individual cubanite grain) and E2 (cubanite and pyrrhotite grains (Fig. 1)) were examined with a 200keV JEOL 2200FS at NRL.

Results: EMPA of the 16 cubanite grains yield an average composition of: 16.3±0.2 at.% Cu, 33.4±0.4 at.% Fe, and 50.3±0.6 at.% S (2σ-deviation). The average composition of the pyrrhotite grains associated with cubanite is: 45.8±0.4 at.% Fe, 0.9±0.2 at.% Ni, and 53.3±0.4 at.% S (2σ-deviation). TEM-EDS analyses agree, within error, with EMPA.

TEM analyses of assemblage E3 reveal a single crystal crosscut by a vein. SAED patterns obtained in three orientations from the bulk cubanite are consistent with the low-temperature orthorhombic form (zone axes: [010], [01-1], and [12-1]) [5]. Secondary reflections are present, in one direction, in the pattern from the [010] zone axis. In comparison, the vein consists of three layers. The outer layer contains Cu, Fe, and S, with higher Cu:S and lower Fe:S ratios than the adjacent cubanite. The interior layer is amorphous and contains Fe-, Ni- and O-bearing material. A Ca-, S-, and O-bearing material occurs in the center of the amorphous region, although not throughout the entire vein.

Assemblage E2 consists of 4 crystalline areas separated by crosscutting veins (Fig. 1c). The largest grain is homogenous at the nm scale. Measurements of cubanite SAED patterns from two orientations are consistent with the low-temperature form. The pattern from the [3-10] axis has secondary spots in two directions and doublets in one (Fig. 1d). The [2-10] zone axis' pattern has secondary spots in one direction. SAED patterns of the other large grain are consistent with 4C monoclinic pyrrhotite [6]. A smaller twinned crystal of 4C monoclinic pyrrhotite ([010] and [110] zone axes) [6-8] is separated from the main pyrrhotite grain. A small Cu-Fe-sulfide grain occurs between the pyrrhotite grains, but it is depleted in Cu and S and enriched in Fe relative to the main cubanite crystal. Its SAED pattern (only obtained from one orientation) is consistent with cubanite ([3-10] zone axis).

The vein material is similar to that described for section E3. The vein cross-cutting the largest cubanite grain is free of Ca-bearing material, whereas that between the main cubanite and pyrrhotite crystals contains all three layers described above. In addition, Hg-sulfide grains are dispersed in the area between the small pyrrhotite grain and the small Cu-Fe-sulfide, as well as below the main cubanite grain.

Discussion and Conclusion: The orthorhombic crystal structure of cubanite constrains the maximum temperature of formation. $CuFe_2S_3$ has two polymorphs: a low-temperature orthorhombic form (cubanite) and a high-temperature cubic form (isocubanite). Cubanite undergoes an irreversible phase transition to isocubanite at 210˚C [9]. Upon cooling below 210˚C isocubanite does not revert to cubanite, but rather exsolves chalcopyrite and pyrrhotite [10-12].

On its own, the presence of 4C monoclinic pyrrhotite is indicative of low temperatures, as it is not stable above ~250˚C [13, and references therein]. The combination of cubanite and 4C pyrrhotite indicate even lower temperatures. They do not form a stable assemblage on the 200˚C Cu-Fe-S ternary diagram [14, 15]. They do, however, have a tie line between them in an extrapolated 25˚C Cu-Fe-S ternary [16]. These crystal structures and temperature constraints are consistent with the petrologic evidence suggesting that CI-chondrite cubanite formed at a later stage than pyrrhotite by precipitating from an aqueous fluid as the parent body cooled [1]. Secondary spots and doublets in the cubanite diffraction patterns could be indicative of a cation superlattice, vacancy ordering, structural varia-

tion, or a partially arrested phase transition. Modeling and experimental work will elucidate this.

The vein material formed after the pyrrhotite and cubanite through aqueous alteration on the parent body and/or during terrestrial weathering. The iron depletion in the outer layer of the vein is consistent with iron being preferentially removed (vis-a-vis copper) from Cu-Fe-sulfides during oxidation or weathering [16]. The Ca-, S-, and O-bearing material is presumably a sulfate which could have formed in situ on the parent body or may be a product of terrestrial weathering [17]. Hg-sulfide in CM chondrites is the product of low temperature aqueous alteration on the parent body [18]; its presence in Orgueil is indicative of low-temperature aqueous processing on the CI-parent body.

Modeling of hydrous asteroids (CM- and CI-like) predicts alteration temperatures of 50-150˚C [19]. Data from oxygen isotopes suggest an alteration temperature of ~150˚C [20]. The presence of 4C monoclinic pyrrhotite and cubanite, as well as mercury sulfide, support the predicted low-temperature alteration for the CI-chondrite parent body. The crystal structures also allow for direct comparison of sulfides from CI chondrites and other extraterrestrial materials, such as Stardust samples.

References: [1] Bullock, E.S. *et al*. (2005) GCA 69, 2687-2700. [2] Macdougall, J.D. and J.F. Kerridge (1977) Science, 561-562. [3] Berger, E.L. *et al.* (2009) LPS XL, 1892. [4] Zega, T.J. *et al.* MAPS 42, 1373-1386. [5] Fleet, M.E. (1971) Z Kristallogr 132, p. 276-287. [6] Tokonami, M. *et al*. (1972) Am Mineral 57, 1066-1080. [7] Putnis, A. (1975) Contrib Miner Petr 52, 307-313. [8] Posfai, M. *et al*. American Mineralogist, 2000. 85: p. 1406-1415. [9] Caye, R. *et al*. (1988) Mineral Mag 52, 509-514. [10] Miyamoto, M. *et al*. (1980) Mater Res Bull 15, 907-910. [11] Pruseth, K.L. *et al*. (1999) Eur J Mineral 11, 471-476. [12] Putnis, A. *et al*. (1977) Phys Chem Miner 1, 335-349. [13] Wang, H. *et al. (2006)* J Sulfur Chem 27, 271-282. [14] Kullerud, G. *et al*. (1969) in *Magmatic Ore Deposits: A symposium*, Economic Geology Publishing Co.: Lancaster, 323-343. [15] Yund, R.A. and G. Kullerud (1966) J Petrol 7, 454. [16] Vaughan, D.J. and J.R. Craig (1997) in *Geochemistry of Hydrothermal Ore Deposits, Third Edition*, John Wiley and Sons: New York, 367-434. [17] Airieau, S.A. *et al. (2005) GCA* 69, 4166-4171. [18] Lauretta, D.S. *et al*. (1999) EPSL 171, 35-47. [19] Zolensky, M.E. and K.L. Thomas (1995) GCA 59, 4707-4712. [20] Clayton, R.N. and T.K. Mayeda (1999) LPS XXX, 1795.

Acknowledgements: Special thanks to the Vatican Observatory for providing samples. This work was supported by NASA grants: NNX09AC60G (DSL) and NNX08AW48H (ELB).

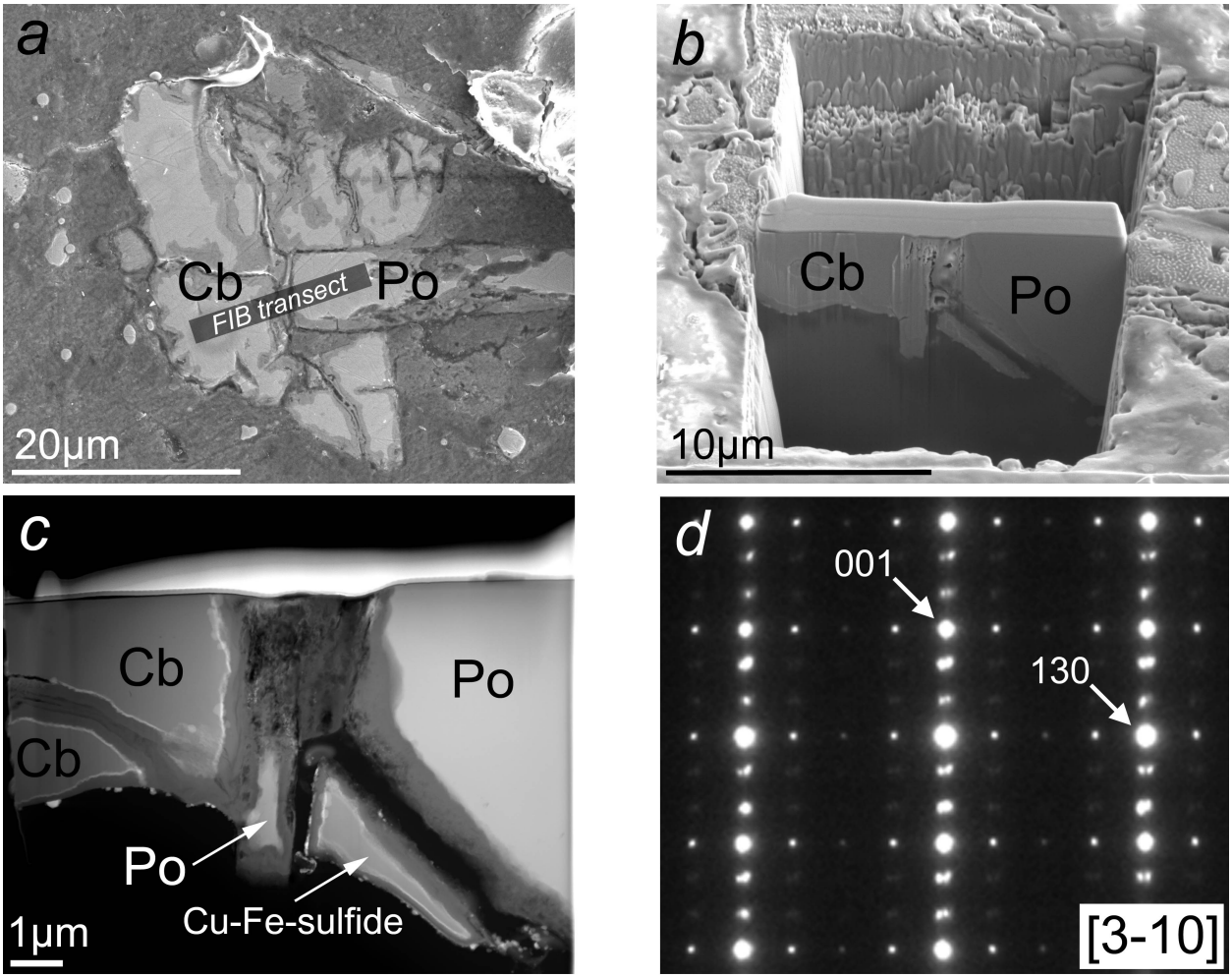

Figure 1. (a) BSE image of cubanite (Cb)/pyrrhotite (Po) assemblage E2. (b) SEI of FIB section preparation. (c) HAADF image of mineral interface. (d) SAED pattern of [3-10] zone axis for orthorhombic cubanite.